Oil Shale, 2017, Vol. 34, No. 2, pp. 181–194
doi: https//doi.org/10.3176/oil.2017.2.07
ISSN 0208-189X

VARIABLE ACTIVATION ENERGY PRINCIPLE TO MODEL OIL SHALE PYROLYSIS KINETICS

OMAR SALIM AL-AYED[(a)*], MOHAMMAD WALEED AMER[(b)], MOHAMMED MATOUQ[(a)]

[(a)] Department of Chemical Engineering, Faculty of Engineering Technology, Al Balqa Applied University, P.O. Box 15008, Marka 11134, Jordan
[(b)] Department of Chemistry, Faculty of Science, University of Jordan, Amman, 11942, Jordan

Abstract. *The oil shale (OS) sample from Sultani mine, southern Jordan, was subjected to thermogravimetric/differential thermogravimetric (TG/DTG) and differential scanning calorimetry (DSC) analysis. Analysis was used to determine the kinetic parameters in the 300–540 °C temperature range, employing different heating rates (3, 5, 10, 20, 30 °C/min). The first order conversion function was found to best represent the oil shale pyrolysis kinetics. The data in the studied pyrolysis temperature range was divided into three zones according to the behavior of the quantity* $\ln(dx/dT/(1-x))$ *vs* $1/T(K)$. *In the first linear zone, the apparent activation energy and frequency factor were found to be in the range of 63.1–94.2 kJ/mol and 9.3E+3–5.03E+6, respectively. In the second zone of analysis, the apparent activation energy was found to be negative and varied between –25.8 and –2.13 kJ/mol and the corresponding frequency factor was in the range of 19.65–0.00098. In the third zone under study, the calculated apparent activation energy and frequency factors were in the range of 186.9–342.1 kJ/mol and 1.87E+12–1.46E+23, respectively.*

Keywords*: oil shale pyrolysis, activation energy, kinetic parameters, differential thermogravimetric analysis.*

1. Introduction

Numerous investigations on oil shale (OS) pyrolysis kinetics have been carried out [1–9]. These studies used experimental methods such as differential thermal (DT), thermogravimetric (TG), Rock-Eval, and triple quadrupole mass spectrometer (TQMS) methods, or a simple laboratory retorting system to predict the conversion of kerogen or rate of mass loss

* Corresponding author: e-mail *omar.alayed@bau.edu.jo*

with pyrolysis temperature. These procedures measure the total weight loss as a function of time and temperature. Different reaction kinetic models, including isothermal, non-isothermal, isoconversional, integral, differential and other methods, have been proposed to treat the experimental data. Some investigators [1–3] developed kinetic models to determine the kinetic equation parameters to predict the conversion or rate of mass loss, while others [4, 5] used the distribution of activation energy (isoconversion) values to test the applicability of their models to oil shale pyrolysis in the temperature range studied. Investigators [8] found that activation energy value increased with increasing heating rate up to 15 °C/min, whereas no such trend was observed with higher heating rates. The nature of oil shale, including its geological formation process, composition, structure, constituents, as well as pyrolysis process and conditions, have a direct impact on the desired end product. However, several thermally produced components are a result of direct and indirect chemical reactions taking place during oil shale pyrolysis, which makes the direct investigation of individual reactions or components a difficult task. Recent studies [5, 10] used the isoconversional method and parameter fitting to analyze the set of data for Green River oil shale to generate the distribution of energy in the 573–773 K temperature range. Coats and Redfern [11] reported the distribution of activation energy values in the range of 95–450 kJ/mol for kerogen and raw oil shale decomposition by using the Friedman method of analysis. The kinetic study is essential for the understanding of the mechanisms of reactions involved in the pyrolysis process to generate the mathematical modeling, which may lead to improved techniques for oil shale conversion.

Kinetic modelling of oil shale or its demineralized kerogen is viewed from different perspectives. Several models [11–14] employed single activation energy value to estimate kinetic parameters, assuming a first order of reaction, whilst other methods [5, 7, 15] made use of the distribution of activation energy values over the entire range of pyrolysis process. The spread of activation energy values over the entire range of conversion characterizes the different, either primary or secondary, reactions of thermal cracking. The low values of activation energy are viewed to correspond to the release of gases such as hydrogen, carbon monoxide, etc., and light hydrocarbons such as C_1–C_3 at low pyrolysis temperatures, and intermediate activation energy values are attributable to decomposition (pyrolysis) of large kerogen molecules in the wide range of temperature, while much higher activation energy values in the end of pyrolysis at higher temperatures are ascribed to the breakage of much stronger bonds. The principle of variable activation energy is more representative for the actual oil shale pyrolysis since its continuous process is composed of several parallel, series, simultaneous, primary and secondary complex reactions. Even the values of activation energy over the entire material conversion and reaction temperature range are dependent on heat input rate and thermal conductivity or physical properties of raw oil shale.

Few studies [15, 16] have identified hydrocarbon components evolved as a result of pyrolysis. These investigations reported individual components or grouped them according to carbon atom number. Tiwari and Deo [16] observed an increase in the quantity of the component produced with increasing heating rate in addition to a slight shift in the reaction temperature range; it was apparent from their results that the product distribution was also altered due to increasing heating rate from 5 to 10 °C/min. A similar trend of changing composition of evolved gases was observed by other workers [17]. In conclusion, the type of evolved hydrocarbons and their quantity changes with heating rate, which is a measure of the heat flux to the material, indicating either the change of the reaction mechanism or occurrence of complex and/or secondary reactions due to higher heat input to oil shale or presence of a catalyzing material, enhance chemical reactions or increase in system voidage.

It is evident from the abovementioned works that a single value of activation energy, which is probably an average value over the entire pyrolysis temperature range, is not appropriate to model the process kinetics, and the distribution of activation energy values would serve the purpose better. The objective of this work is to model the pyrolysis kinetics of Jordanian Sultani oil shale through applying the differential method of analysis and introducing negative activation energy, which is supported by differential scanning calorimetry (DSC) heat interactions.

2. Experimental

In the present work, the oil shale sample from Sultani mine, southern Jordan, was used. A sufficient quantity of oil shale was transported from the mine to the laboratory. The sample was crushed and a representative portion of it was selected for the study. The test sample was prepared to be less than 200 μ in size for thermal gravimetric study. The Fischer Assay analysis results are presented in Table 1. The thermogravimetry/differential thermogravimetry (TG/DTG) curves were produced by a NETZSCH TG 209F1 equipment (Germany) with a 100 ml/min nitrogen flow rate. The employed heating rates were 3, 5, 10, 20, and 30 °C/min. The TG/DTG runs were conducted from ambient temperature to 550 °C and the results are shown in Figure 1. In this work, the kinetics of oil shale pyrolysis was based on the total weight loss between 300 and 540 °C calculated from the thermograms curves. The total mass loss was recalculated from the TG curves for each run. The total mass loss in the prescribed temperature interval was recalculated from the generated data by summing up the rates of mass loss in the entire selected temperature range, which must be equal to the value calculated directly from the thermogram curves, otherwise the results will be misleading. The conversion x was calculated as mass loss at any time divided by total mass loss between 300 and 540 °C.

The percent total mass loss and the percent mass loss between 300 and 540 °C for all runs are presented in Table 2. The percent total mass loss of samples increased from 23 to 27% with increasing heat input to them. A similar trend was observed for the percent mass loss in the hydrocarbon evolution region characterized by the 300–540 °C temperature range.

Table 1. Fisher Assay analysis of Sultani oil shale sample, wt%

Total water	Total oil	Spent shale	Gas loss
1.94	9.45	85.41	3.2

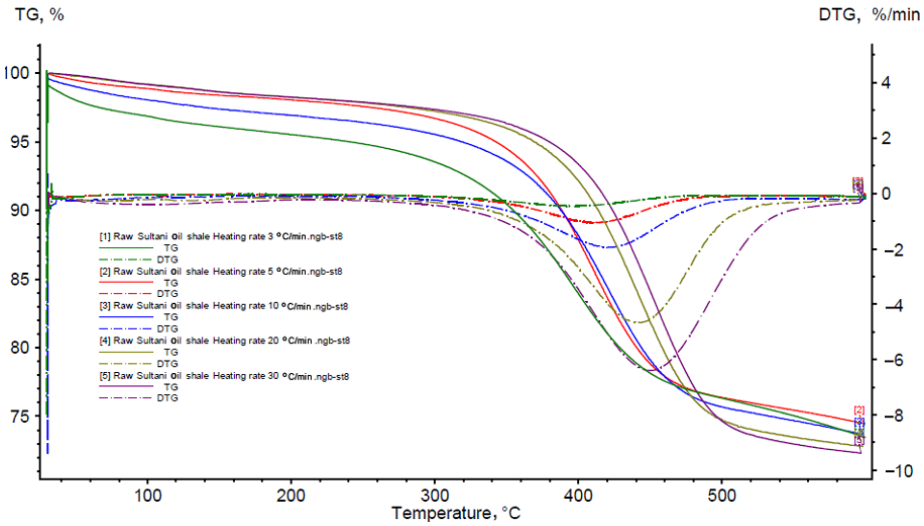

Fig. 1. TG and DTG curves for Sultani oil shale sample.

Table 2. Sample mass loss at the studied heating rates and pyrolysis temperature range

Heating rate h, °C/min	3	5	10	20	30
Percent total mass loss	23.20	24.08	24.39	26.22	26.75
Percent mass loss between 300 and 540 °C relative to total loss	78.54	87.56	84.72	89.87	90.38

3. Kinetic model development

Some of the reported studies [18–20] on oil shale modelling have employed first order kinetics as indicated in Equation (1):

$$\frac{dx}{dt} = k(1-x)^n. \tag{1}$$

The conversion function, x, is defined as shown in Equation (2):

$$x = (m_o - m_t)/(m_o - m_f), \tag{2}$$

where m is the mass, subscripts o indicate the initial time at 300 °C, subscript t represents any time during run, f denotes the final pyrolysis temperature, n is the reaction order and can take values 0.5, 1, 1.5 and 2. Introducing the heating rate, h, °C/min, into Equation (1) leads to Equation (3):

$$\frac{dx}{dT} = \frac{k_o}{h}\exp(-E/RT)(1-x)^n. \tag{3}$$

The differential Equation (3) can be rearranged for kinetic modelling as follows:

$$\ln(dx/dT/(1-x)^n) = \ln(k_o/h) - E/RT. \tag{4}$$

First of all, Equation (4) is used to determine the most appropriate value of reaction order, n. Equation (4) results in a plot between the left-hand side and the inverse of pyrolysis temperature on the right-hand side. Upon determining the best value of the reaction order, a plot of the left-hand side on the y-axis against the inverse of pyrolysis temperature in Kelvin would result in determination of the kinetic parameters, i.e. the pre-exponential factor k_o from the intercept and the activation energy of the system from the slope of the line obtained from data fitting.

4. Results and discussion

The data obtained from TG/DTG at heating rates of 3, 5, 10, 20 and 30 °C/min are shown in Figure 1. As seen from the figure, the sample loss percent decreased with increasing heating rate unlike the sample loss percent at the same pyrolysis temperature up to 480–490 °C, while above this temperature range, the lower heating rates resulted in the lower weight loss percent against that at higher heating rates. Although this trend is true, the total mass loss percent increased with increasing heating rate as indicated in Table 2. The DTG data, %/min, i.e. the derivative of the TG curve, is higher for a higher heating rate.

The DTG data for each run was used to recalculate the conversion as presented in Equation (2) for kinetic modelling. Introducing the heating rate, dT/dt, into Equation (1) and rearranging it led to Equation (3), which is the differential form of a standard procedure to model kinetics and determine the parameters. Although the reaction order was assumed to be one during the entire kinetic analysis, Equation (4) was used to check the validity of this assumption by determining n as shown in Figure 2. As indicated in Figure 2, the plot of the left-hand side of Equation (4) vs inverse of pyrolysis

temperature for different values of n, i.e. 0.5, 1.0, 1.5 and 2.0, resulted in selection of reaction order to be equal to one, the most appropriate since the R-squared value was 0.9952.

The generated dx/dT and the calculated conversion x were fitted to Equation (4). Figure 3 shows the family of generated curves for the studied heating rates. As can be seen from this figure, the curve is not a straight line, i.e. the relationship between the quantities $\ln(dx/dT/(1-x))$ and inverse of pyrolysis temperature is not amenable to linear kinetics in the entire pyrolysis temperature range. As a result of this behavior, the curve is divided into three zones.

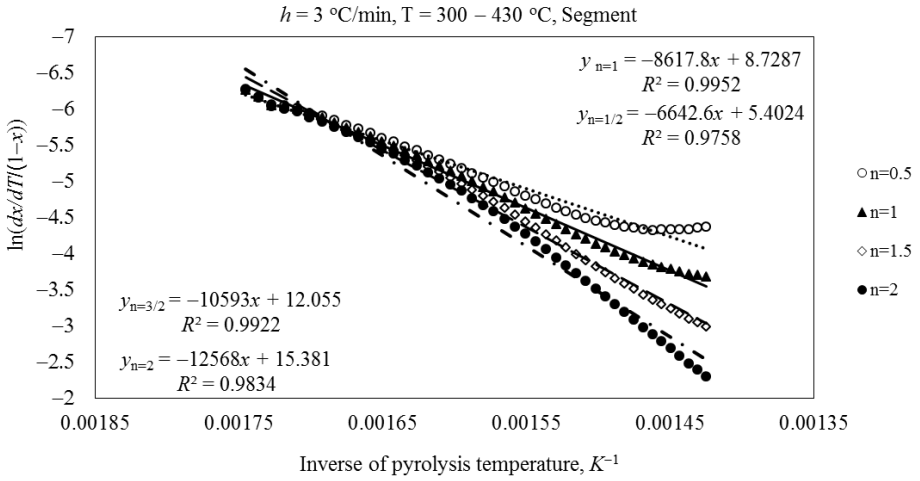

Fig. 2. Reaction order determination.

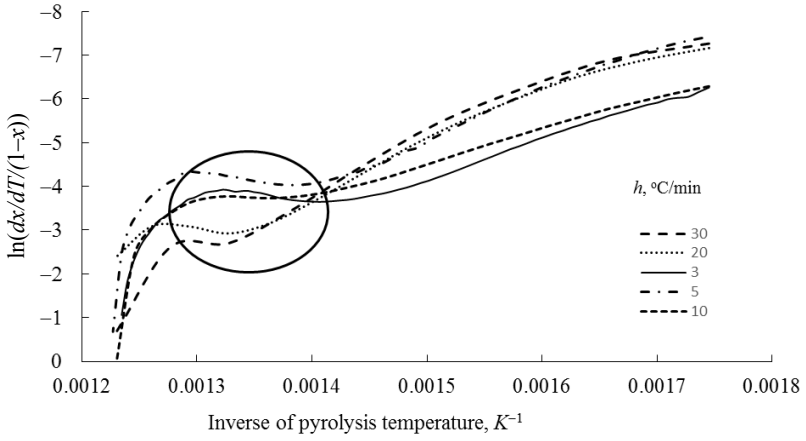

Fig. 3. Natural logarithm of ($dx/dT/(1-x)$) vs inverse of pyrolysis temperature, experimental data at heating rates of 3, 5, 10, 20 and 30 °C/min.

4.1. First increasing range region

The division of the curve into three different segments is shown in Figure 3. The first zone is a linear range where $\ln(dx/dT/(1-x))$ increased with increasing pyrolysis temperature from 300 to 480 °C or in the vicinity of this temperature depending upon heating rate value. The higher the heating rate is, the higher the end temperature of the linear range is. In the second zone, the right-hand side of Equation (4) decreased with increasing temperature and this behavior is covered by the 440–510 °C temperature range depending upon heating rate. Finally, the third zone of the curve is characterized by a steep rise in the temperature-heating rate relationship between 490–540 °C, while this range may vary with the selected heating rate.

The data in Table 3 presents the range in which the increments for all heating rates increased with temperature. As indicated in the table, considering the linear segment, the calculated activation energy in this region increased from 71.7 to 89.1 kJ/mol when the heating rate increased from 3 to 5 °C/min. At the same time, a decrease in the calculated activation energy from 89.1 to 63.1 kJ/mol at the heating rates of 5 and 10 °C/min and an increase from 89.1 to 89.97 kJ/mol at 10 and 20 °C/min and, finally, an increase to 94.20 kJ/mol at 30 °C/min can be observed. It is clear that the distribution of activation energy in the first zone is a function of heating rate and pyrolysis temperature. The frequency factors associated with evaluated activation energies are presented in Table 3. The existence of a strong correlative relationship of this factor with activation energy is well known and it is assumed that the frequency factor is a weak function of the reaction temperature. Hence, it can be concluded that variable activation energy models the process kinetics.

Table 3. The negative slope of the linear range of Figure 2 curves

Heating rate h, °C/min	3	5	10	20	30
Temperature range, °C	300–430	300–342	300–440	300–460	300–480
Apparent activation energy, kJ/mol	71.7	89.1	63.1	89.97	94.2
Frequency factor k_o	1.85E+4	3.0E+5	9.5E+3	1.67E+6	5.03E+6

4.2. Decreasing range region

The second segment of the curve in Figure 3 is characterized by a decrease in $\ln(dx/dT/(1-x))$ with increasing pyrolysis temperature. The decreasing $\ln(dx/dT/(1-x))$ with increasing pyrolysis temperature results in a positive slope of the curve as shown in the circulated region of Figure 3. The decreasing portion is more magnified at lower heating rates than at higher heating rates due to the large number of experimental points plotted, and a wider temperature range. Because of this behavior, the calculated slope of the straight line of this region would be positive, resulting in a negative activation energy value. Mozurkewich and Benson [21] have thoroughly discussed

the concept of occurrence of negative activation energy in some chemical reactions. The temperature range and the corresponding estimated negative activation energy values obtained in this study are presented in Table 4. As can be seen from the table, the estimated values of negative activation energy varied between –30 and –2.13 kJ/mol. The frequency factor magnitudes calculated corresponding to these negative activation energy values are also presented in Table 4. The values of the pre-exponential factor ranged from 0.00098 to 19.65, which indicates the independence of the implicit correlative effect of the negative activation energy. This behavior is in agreement with the observed weak k_o-E(positive) relationship, i.e. the higher the activation energy value, the higher the magnitude of the frequency factor. The trendline of the data and the degree of fit or the R-squared values are depicted in Figure 4.

Table 4. The positive slope of the second zone of Figure 2 curves

Heating rate h, °C/min	3	5	10	20	30
Temperature range, °C	440–490	450–500	450–490	490–520	490–520
Apparent activation energy, kJ/mol	–25.8	–30.4	–4.41	–2.13	–14.28
Frequency factor k_o	9.84E–4	5.7E–4	0.477	1.3	19.65

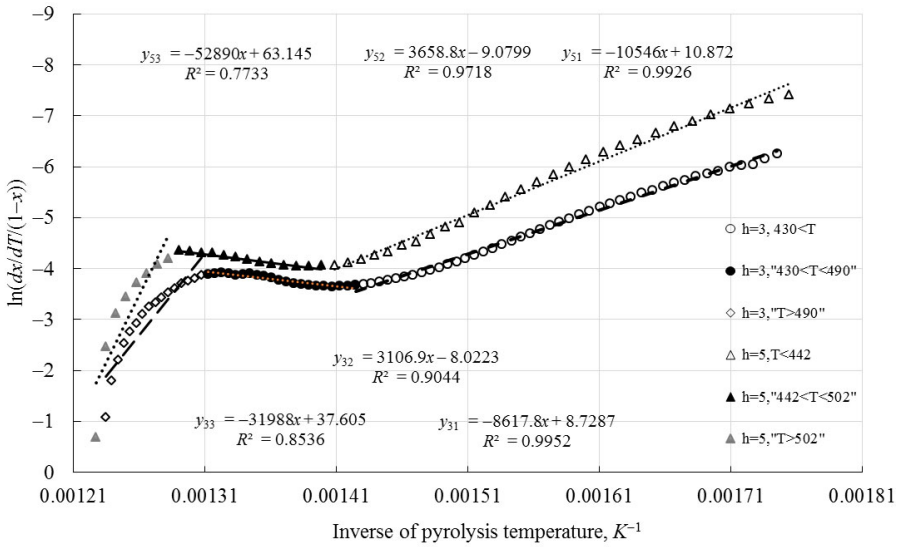

Fig. 4. Fitting 3 and 5 °C/min heating rates to data and R-squared values. (In y_{ij} "i" stands for "h" and "j" for "zone".)

4.2.1. Negative activation energy

As mentioned above, the calculated activation energy value was negative, hence, the justification and explanation are necessary and required**.** This concept was applied to oil shale kinetic study for the first time. The principle

of negative activation energy has been reported and discussed by several investigators before [21–26]. It is an unrecognized fact that some chemical reactions proceed more slowly at higher reaction temperatures and therefore effectively comply with negative activation energy. Revell and Williamson [22] have suggested a mathematical procedure to explain this phenomenon in chemical kinetics. The justification of negative activation energy will be adopted for oil shale pyrolysis kinetics in the respective region. The complex chemical reactions (thermal or catalyzed) occurring during oil shale pyrolysis, which are possibly composed of series, parallel, elementary and non-elementary, reversible and irreversible reactions, lead to hydrocarbons evolution. If a positive activation energy prevents a reaction from occurring until that amount of energy is provided from the surrounding, then a negative activation energy would imply that the reaction could not be stopped from occurring. The reactants already have plenty of energy for the reaction to occur, so the only way to prevent it from taking place would be to keep the reactants apart [26] or increase the reaction temperature to reduce the collision probability.

Revell and Williamson [22] proposed that the mechanism of an individual pyrolysis reaction obeyed an elementary rate law consistent with the molecularity of the reaction and conformed to the Arrhenius behavior with positive activation energy. The equilibrium constant, K, for an arbitrary reaction taking place during pyrolysis is related to the Gibbs free energy as follows:

$$K = \exp(-\Delta G^o / RT). \tag{5}$$

Equation (5) can be rewritten with the help of the thermodynamic dependency of the molar Gibbs free energy on molar enthalpy and molar entropy as follows:

$$G(p,T) = H - TS. \tag{6}$$

Rewriting the equilibrium constant in Equation (6) we get Equation (7):

$$K = \exp(\Delta S^o / R)\exp(-\Delta H^o / RT). \tag{7}$$

For the rate determining step of an arbitrary reaction, either primary or secondary, which takes place and gives final products during pyrolysis, the rate constant can be written as:

$$k = k^* \exp(\Delta S^o / R)\exp[-(E^* + \Delta H^o) / RT]. \tag{8}$$

When Equation (8) is compared with the standard Arrhenius equation, i.e. $k = k_o \exp(-E / RT)$, we find that the following quantities are identical:

$$k_o = k^* \exp(\Delta S^o / R) \tag{9}$$

and

$$E = E^* + \Delta H^o . \tag{10}$$

Equations (9) and (10) could provide information about the net entropy and net enthalpy of the reacting system during pyrolysis. Equation (10) could lead to the clue of the negative activation energy observed in our calculations, if net ΔH_o is negative for an exothermic single or set of ongoing chemical reaction(s) during pyrolysis, and since E^* is intrinsically positive for the system but $|\Delta H^o| > E^*$, then the apparent activation energy, E, would be negative. The negative activation energy reactions are considered to block to a lesser extent the reactions whose progress depends upon the availability of the reacting materials, while increasing the temperature reduces the collision of the reacting molecules which produce the desired end products, hence reducing the rate. In such a reacting atmosphere, it is possible that the activated complex is more stable than the reactant, which implies negative activation energy. It is quite a clear discussion and supportive to accept negative activation energy existence and justification. Furthermore, the literature findings support the DSC results obtained in this work at a 10 °C/min heating rate as shown in Figure 5. From the figure it can be seen that the exothermicity behavior of the sample is monitored at temperatures between 420 and 488 °C, whereas the negative activation energy value (–4.41 kJ/mol) obtained in this work at the above heating rate is reported in the 450–490 °C temperature range, which corresponds (probably inadvertently) with the exothermicity behavior of the sample, as shown in the DSC curve in Figure 5. It is generally known that the temperature range in which the reported activation energy values are negative is flexible within a margin, depending upon heating rate. The corresponding frequency factor values associated with the reported negative activation energy values are also presented in Table 4.

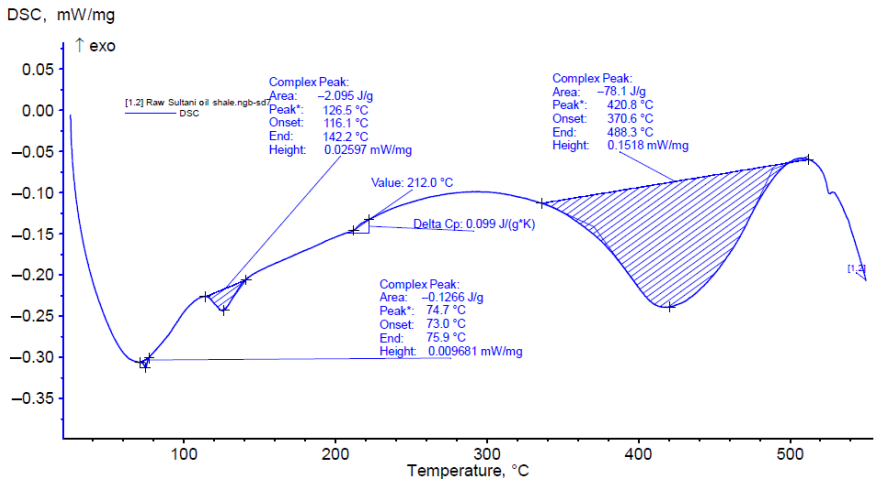

Fig. 5. DSC, mW/mg, with pyrolysis temperature showing the exothermic heat of reaction in the negative activation energy region.

4.3. Second increasing range region

In the second increasing range region in the third zone, the reaction rate bounces back to a sharp increase with increasing pyrolysis temperature after a decreasing region as depicted earlier in Figure 3. This region of pyrolysis is characterized by low reaction rate due to the depletion of the reacting material and high activation energy requirement to break C–O and C–C aliphatic bonds [27, 28]. Generally, no pyrolysis reactions are observed at temperatures higher than 540 °C, depending upon the type of oil shale. As can be seen from Table 5, the relative values of activation energy and the corresponding frequency factor values are very high compared with those obtained earlier in this work for the second and third zones. The activation energy fluctuated from 186.9 to 342.1 kJ/mol, whereas the corresponding frequency factor varied from 1.87E+12 to 1.46E+23. Some researchers [29, 30] ascribed the high apparent activation energy mainly to the much stronger bond breakage such as aromatization of alicyclic compounds, dehydrogenation and combination of aromatic rings, and rupture of heterocyclic compounds. It is well known [28] that increasing the heating rate increases the density of the generated shale oil liquid. This is in agreement with the increased production of heavy components at high pyrolysis temperatures. The findings of the present study are in accordance with these statements.

Table 5. The negative slope of the third zone of Figure 2 curves

Heating rate h, °C/min	3	5	10	20	30
Temperature range, °C	490–540	500–540	490–540	520–540	490–540
Apparent activation energy, kJ/mol	265.95	281.9	204.11	186.92	342.13
Frequency factor k_o	6.44E+16	4.83E+17	1.50E+17	1.87E+12	1.46E+23

5. Conclusions

In this work, the differential method of analysis was applied to Jordanian Sultani oil shale sample. Thermogravimetry/differential thermogravimetry were used to calculate the kinetic parameters – the apparent activation energy and frequency factor. The reaction was determined to be first order. The pyrolysis of oil shale was studied in the temperature range of 300–540 °C. The fitted data were divided into three zones and for each zone the kinetic parameters were determined. A new concept of negative apparent activation energy was employed for the first time and found to be part of the differential method of analysis, which could be appropriate to model the kinetics of oil shale pyrolysis. The findings of this work were supported by the results of differential scanning calorimetry heat interactions obtained.

List of abbreviations

DTG Differential thermogravimetric
DSC Differential scanning calorimetry
E Apparent activation energy, kJ/mol
G Gibbs free energy, J/mol
h Heating rate, °C/min
H Enthalpy, J/mol
K Equilibrium constant
n Reaction order
R Universal gas constant, 8.314 J/K mol
S Entropy, J/mol K
T Temperature, K
TG Thermogravimetric
x Conversion function

Acknowledgement

This project was funded by the "Support to Research, Technological Development & Innovation in Jordan" (SRTD – II), an EU funded project managed by the Higher Council for Science & Technology. Jordan.

The authors would like to express their thanks to The Higher Council for Science and Technology, SRTD II project implementation office for their help, facilities and follow-up during the project period.

REFERENCES

1. Charlesworth, J. M. Oil shale pyrolysis. 2. Kinetics and mechanism of hydrocarbon evolution. *Ind. Eng. Chem. Proc. Des. Dev*., 1985, **24(**4), 1125–1132.
2. Skala, D., Kopsch, H., Sokić, M., Neumann, H. J., Jovanović, J. A. Kinetics and modelling of oil shale pyrolysis. *Fuel*, 1990, **69**(4), 490–496.
3. Johannes, I., Kruusement, K., Veski, R. Evaluation of oil potential and pyrolysis kinetics of renewable fuel and shale samples by Rock-Eval analyzer. *J. Anal. Appl. Pyrol*., 2007, **79**(1–2), 183–190.
4. Al-Ayed, O. S., Matouq, M., Anbar, Z., Khaleel, A. M., Abu-Nameh, E. Oil shale pyrolysis kinetics and variable activation energy principle. *Appl. Energ.*, 2010, **87**(4), 1269–1272.
5. Tiwari, P., Deo, M. Detailed kinetic analysis of oil shale pyrolysis TGA data. *AIChE J*., 2012, **58**(2), 505–515.
6. Li, S., Yue, C. Study of pyrolysis kinetics of oil shale. *Fuel*, 2003, **82**(3), 337–342.
7. Al-Ayed, O. S. Variable reaction order for kinetic modeling of oil shale pyrolysis. *Oil Shale*, 2011, **28**(2), 296–308.
8. Torrente, M. C., Galan, M. A. Kinetics of the thermal decomposition of oil shale from Puertollano (Spain). *Fuel*, 2001, **80**(3), 327–334.
9. Al-Harahsheh, M., Al-Ayed, O., Robinson, J., Kingman, S., Al-Harahsheh, A., Tarawneh, K., Saeid, A., Barranco, R. Effect of demineralization and heating

rate on the pyrolysis kinetics of Jordanian oil shales. *Fuel Process. Technol.*, 2011, **92**(9), 1805–1811.
10. Pan, L., Dai, F., Huang, J., Liu, S., Li, G. Study of the effect of mineral matters on the thermal decomposition of Jimsar oil shale using TG-MS. *Thermochim. Acta*, 2016, **627–629**, 31–38.
11. Coats, A. W., Redfern, J. P. Kinetic parameters from thermogravimetric data. *Nature*, 1964, **201**(4914), 68–69.
12. Flynn, J. H., Wall, L. A. Initial kinetic parameters from thermogravimetric rate and conversion data. *J. Polym. Sci. Part C: Polym. Lett.*, 1967, **5**(2), 191–196.
13. Ozawa, T. Estimation of activation energy by isoconversion methods. *Thermochim. Acta*., 1992, **203**, 159–165.
14. Kissinger, H. E. Reaction kinetics in differential thermal analysis. *Anal. Chem*., 1957, **29**(11), 1702–1706.
15. Greenwood, P. F., George, S. C. Mass spectral characteristics of C_{19} and C_{20} tricylcic terpanes detected in Latrobe Tasmanite oil shale. *Eur. J. Mass Spectrom*., 1999, **5**(3), 221–230.
16. Tiwari, P., Deo, M. Compositional and kinetic analysis of oil shale pyrolysis using TGA-MS. *Fuel*, 2012, **94**, 333–341.
17. Campbell, J. H., Koskinas, G. J., Gallegos, G., Gregg, M. Gas evolution during oil shale pyrolysis. 1. Nonisothermal rate measurements. *Fuel*, 1980, **59**(10), 718–726.
18. Braun, R. L., Rothman, A. J. Oil-shale pyrolysis: kinetics and mechanism of oil production. *Fuel*, 1975, **54**(2), 129–131.
19. Han, H., Zhong, N. N., Huang, C. X., Zhang, W. Pyrolysis kinetics of oil shale from northeast China: Implications from thermogravimetric and Rock-Eval experiments. *Fuel*, 2015, **159**, 776–783.
20. Pan, L., Dai, F., Li, G., Liu, S. A TGA/DTA-MS investigation to the influence of process conditions on the pyrolysis of Jimsar oil shale. *Energy*, 2015, **86**, 749–757.
21. Mozurkewich, M., Benson, S. W. Negative activation energies and curved Arrhenius plots. 1. Theory of reactions over potential wells. *J. Phys. Chem.-US*, 1984, **88**(25), 6429–6435.
22. Revell, L. E., Williamson, B. E. Why are some reactions slower at higher temperatures? *J. Chem. Educ*., 2013, **90**(8), 1024–1027.
23. Strausz, O. P., Connor, J., Van Roodselaar, A., Fair, R. W. Addition of group VIa atoms to tetramethylethylene. Addition reaction with a negative activation energy. *J. Am. Chem. Soc.*, 1971, **93**(2), 560–562.
24. Cunningham, D. A. H., Vogel, W., Haruta, M. Negative activation energies in CO oxidation over an icosahedral $Au/Mg(OH)_2$ catalyst. *Catal. Lett.*, 1999, **63**(1), 43–47.
25. Han, X., Lee, R., Chen, T., Luo, J., Lu, Y., Huang, K. W. Kinetic evidence of an apparent negative activation enthalpy in an organocatalytic process. *Sci. Rep.*, 2013, **3**, Article number 2557.
26. Logan, S. R. *Fundamentals of Chemical Kinetics*. Longman: Harlow, England, 1996, 49–50.
27. Braun, R. L., Rothman, A. J. Oil-shale pyrolysis: kinetics and mechanism of oil production. *Fuel*, 1975, **54**(2), 129–131.
28. Al-Ayed, O. S., Al-Harahsheh, A., Khaleel, A. M., Al-Harahsheh, M. Oil shale pyrolysis in fixed-bed retort with different heating rates. *Oil Shale*, 2009, **26**(2), 139–147.

29. Orr, W. L. Kerogen/asphaltene/sulfur relationships in sulfur-rich Monterey oils. *Org. Geochem*., 1986, **10**(1–3), 499–516.
30. Eglinton, T. I., Sinninghe Damsté, J. S., Kohnen, M. E. L., de Leeuw, J. W., Larter, S. R., Patience, R. L. Analysis of maturity-related changes in the organic sulfur composition of kerogens by flash pyrolysis-gas chromatography. In: *Geochemistry of Sulfur in Fossil Fuels* (Orr, W. L., White, C. M., eds.), ACS Symposium Series, 429. Washington DC, 1990, 529–565.

Presented by J. Kann
Received June 17, 2016